Quantum mechanical and spectroscopic (FT-IR, 13C, 1H NMR and UV) investigations of 2-(5-(4-Chlorophenyl)-3-(pyridin-2-yl)-4, 5-dihydropyrazol-1-yl)benzo[d]thiazole by DFT method

ARTICLE · MARCH 2014

READS
11

1 AUTHOR:

Diwaker Kumar
Indian Institute of Technology Mandi
23 PUBLICATIONS **41** CITATIONS

SEE PROFILE

Spectrochimica Acta Part A: Molecular and Biomolecular Spectroscopy 128 (2014) 819–829

Contents lists available at ScienceDirect

Spectrochimica Acta Part A: Molecular and Biomolecular Spectroscopy

journal homepage: www.elsevier.com/locate/saa

Quantum mechanical and spectroscopic (FT-IR, ^{13}C, ^{1}H NMR and UV) investigations of 2-(5-(4-Chlorophenyl)-3-(pyridin-2-yl)-4, 5-dihydropyrazol-1-yl)benzo[d]thiazole by DFT method

Diwaker *

School of Basic Sciences, Indian Institute of Technology Mandi, Mandi, HP 175001, India

HIGHLIGHTS

- Theoretical vibrational and NMR spectra is investigated.
- Electrostatic potential for the title compound is calculated.
- Structural parameters are investigated theoretically and compared with the experimental values.
- The absorption spectra is calculated in solvent environment.
- HOMO–LUMO analysis is performed to study the band gap related properties.
- The PED calculation is done to assign wavenumbers.
- NBO analysis is also performed.

GRAPHICAL ABSTRACT

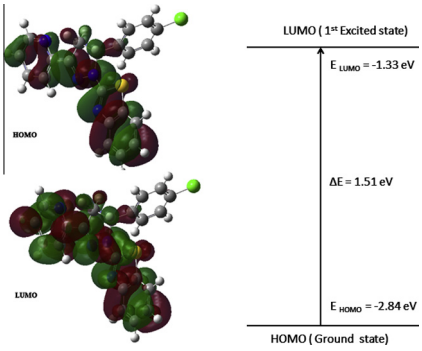

ARTICLE INFO

Article history:
Received 10 December 2013
Received in revised form 27 February 2014
Accepted 27 February 2014
Available online 15 March 2014

Keywords:
DFT
HOMO–LUMO
B3LYP
MEP
GIAO

ABSTRACT

The electronic, NMR, vibrational, structural properties of a new pyrazoline derivative: 2-(5-(4-Chlorophenyl)-3-(pyridine-2-yl)-4,5-dihydropyrazol-1-yl)benzo[d]thiazole has been studied using Gaussian 09 software package. Using VEDA 4 program we have reported the PED potential energy distribution of normal mode of vibrations of the title compound. We have also reported the ^{1}H and ^{13}C NMR chemical shifts of the title compound using B3LYP level of theory with 6-311++G(2d,2p) basis set. Using time dependent (TD-DFT) approach electronic properties such as HOMO and LUMO energies, electronic spectrum of the title compound has been studied and reported. NBO analysis and MEP surface mapping has also been calculated and reported using ab initio methods.

Introduction

The title compound shows experimentally well proven sensing properties for selective detection of Fe^{3+} ions in mixed aqueous media [1]. In the literature, there has been keen interest in the development of sensors based upon fluorescent techniques for detection of various metals ions [2], however literature survey also reveals very few ab initio HF/MP2/DFT calculations of such type of compounds. Fluorescence is a simple, sensitive, non-destructive, and convenient characterization technique for detection of very small amount (in ppm) of metal ions in solutions. As an important physiologically important ion, Fe^{3+} ions plays a very important role at the cellular level [3] and its deficiency can induce a variety of

* Tel.: +91 9736660660.
E-mail address: diwakerphysics@gmail.com

http://dx.doi.org/10.1016/j.saa.2014.02.196
1386-1425/

diseases [4], hence the determination of traces of iron in environmental and industrial samples has been an important topic in different type of analysis. In the interest of such applications the quantum mechanical calculations of the title compound are thoroughly investigated. The aim of this work is to predict the structural, electronic, vibrational spectral parameters and other molecular properties apart from sensing applications of the title compound using ab initio approach [5–9].

Computational methods

DFT has proved to be extremely useful in treating the electronic structures of molecules. Calculations of the new 2-(5-(4-Chlorophenyl)-3-(pyridin-2-yl)-4,5-dihydropyrazol-1-yl)benzo[d]thiazole is carried out with Gaussian 09 program [10] using B3LYP level of theory and 6-311G++(2d,2p) basis set to predict the optimized ground state geometry of the molecule. Optimized parameters of the pyrazoline derivative are given in Table 1 and are compared with the experimental values. Optimized structural parameters are used in the isotropic chemical shifts, vibrational frequency and electronic property calculations. The nuclear magnetic resonance (NMR) chemical shift calculations are performed using Gauge-Invariant Atomic Orbital (GIAO) [11,12] method at B3LYP level using 6-311++(2d,2p) basis set. Solvent effect on theoretical NMR parameters is included using Conductor Polarizable Continuum Model (CPCM) [13] provided by Gaussian 09 program. Chloroform is used as a solvent. Time dependent DFT method (TD-B3LYP) on the ground state optimized geometry is used to calculate the excited states and the electronic transitions. In order to produce the electronic spectra, excitation energies for the singlet and triplet states have been calculated. To understand the planar or non-planar structure of the molecule potential energy scan has been performed. HOMO LUMO is calculated at B3YLP level of theory using 6-311++G(2d,2p) basis set. The theoretical vibrational spectrum of the title compound is interpreted by means of Potential energy Distribution (PED) using VEDA 4 program. The NBO analysis [14] is performed using NBO program at B3LYP/6-311++G(2d,2p) level in order to understand various interactions between the filled and the vacant orbitals. MEP surface is plotted to reveal the chemical reactivity of the molecule. The structure of the title compound is shown in Fig. 1.

Results and discussion

Structural parameters

The ground state geometry of the new pyrazoline derivative is investigated theoretically by performing a DFT calculation using the Becke3-Lee–yang-Parr hybrid functional (B3LYP) [15] with 6-311++G(2d,2p) basis set. The geometry is fully optimized with tight convergence criteria and the structure is local minima on the PES. One can conclude that our calculation is successful, as the difference between calculated and experimental bond lengths, bond angles is of few Å. Fig. 1 (supplementary information) represents the stable conformation of the title compound calculated using DFT theory. We have compared our calculated values with the experimentally obtained results by other authors and found that our results for the optimized ground state geometry of the title compound are in close agreement with the experimentally obtained thereby proving DFT method a valuable tool to predict various molecular properties. The selected calculated bond lengths (R), angles (Å) for the title compound using DFT/B3LYP/6-311++G(2d,2p) level of theory along with their corresponding experimental values are listed in Table 1.

Correlation R^2 values [16] between the calculated and the experimental parameters of bond lengths for the title compound is shown in Fig. 2 and found to be 0.9932.

Frontier molecular orbitals

Chemical reactivity of a molecule can be determined from the HOMO–LUMO band gap. HOMO–LUMO band gap plays a very important role in determining the chemical reactivity, stability of the molecule [17], UV–Vis spectra, chemical reactions, electrical properties and optical properties. LUMO energy means ability to accept an electron while HOMO energy means ability to donate an electron. Chemical reactivity of a molecule can be determined from the HOMO–LUMO band gap. A small band gap implies low kinetic stability of the molecule. HOMO–LUMO separation is a result of significant degree of intermolecular charge transfer from the electron donor groups to the electron acceptor groups through π conjugated paths. Energy gap between HOMO and LUMO has also been used to prove the bioactivity from intramolecular charge transfer (ICT). The calculations indicate that title compound has (859) molecular orbitals out of which (101) are occupied molecular orbitals while rest are virtual molecular orbitals. Out of these (101) and (102) are the HOMO and LUMO molecular orbitals. The HOMO lying at −2.84 eV (computed by TD-DFT) and the LUMO is lying at −1.33 eV. If we divide the molecule into two parts at bond length (C20—C21/C8—C16) we noticed that the HOMO–LUMO distribution is mainly at the lower end of the molecule in the rings containing nitrogen and sulphur atoms, however there is no distribution on the top part of molecule in which a ring is attached to the chlorine atom. HOMO electrons are mostly localized on the rings having nitrogen atom. On the other hand LUMO electrons are mainly localized on the rings having presence of both sulphur and nitrogen atom. Both HOMO and LUMO are mostly localized on rings which show that they are π type orbitals. HOMO (orbital 101) → LUMO (orbital 102) transition implies an ED transfer in between benzene rings to ($\pi \rightarrow \pi^*$) transition. The energy gap is found to be 1.51 eV, which implies that title molecule has high kinetic susceptibility and low chemical reactivity. Large band gap also makes the title compound suitable for wide range of applications such as solar cell applications and many more. The HOMO LUMO for the title compound are shown in Fig. 2 (supplementary information).

Chemical shifts: ^{1}H and ^{13}C NMR spectra

NMR spectroscopy is currently used for the structural and functional determination of the molecules. The chemical shifts of the title compound have been calculated using the Gaussian 09 program package. The calculated ^{1}H and ^{13}C NMR chemical shifts of the title compound together with the corresponding experimental values are shown in Table 2 and Table 3 as values relative to tetramethylsilane. ^{1}H and ^{13}C NMR chemical shifts were computed using the gauge-independent atomic orbital (GIAO)/B3LYP/6-311++G(2d,2p) method [18] in chloroform as solvent. The ^{1}H NMR spectra of the title compound in chloroform shows a multiplet peaks in the range (8.58–8.60) ppm for Aromatic CH. Corresponding calculated values lies at (9.00) ppm. Similarly there are other multiplet peaks for aromatic CH which lies in the range (8.17–8.19) ppm, (7.65) ppm, (7.25–7.32) ppm, (7.09–7.14) ppm respectively while the corresponding calculated value are at (8.99) ppm, (8.11) ppm, (7.47–7.89) ppm and (7.65) ppm respectively. Other peaks in the ^{1}H NMR spectra of the title compound is a doublet at (7.76) ppm while the corresponding calculated value is at (8.19) ppm. The ^{1}H NMR spectra of the title compound in chloroform also shows double doublet for pyrazoline-H at (5.80) ppm, (4.09) ppm and (3.49) ppm respectively while the corresponding calculated values are at (5.58) ppm (4.31) ppm and (3.47) ppm respectively. The ^{13}C NMR spectra of the title compound in chloroform shows peaks in the range from (43.29–162.89) ppm while the corresponding calculated values are in the range from (46.60–167.94) ppm. For C22 and

Table 1
Optimized geometrical parameters of the title compound at (DFT/B3LYP/6-311++G(2d,2p).

Bond length (Angstrom)			Bond angles (degrees)			Dihedral angles (degrees)		
	Exp (Ref. [1]*)	Calculated		Exp (Ref. [1]*)	Calculated		Exp (Ref 1*)	Calculated
C1—C6	1.389	1.388	C6—C1—C2	121.32	121.97	C6—C1—C2—N1	−177.92	−179.99
C1—C2	1.397	1.410	C6—C1—S1	128.99	128.81	C6—C1—C2—C3	1.50	0.14
C1—S1	1.747	1.755	C2—C1—S1	109.67	109.20	S1—C1—C2—N1	0.80	0.41
C2—N1	1.390	1.381	N1—C2—C3	124.66	125.11	N1—C2—C3—C4	178.29	178.91
C2—C3	1.396	1.397	N1—C2—C1	115.86	115.92	S1—C1—C2—C3	−179.73	−179.72
C3—C4	1.378	1.390	C3—C2—C1	119.47	121.97	C1—C2—C3—C4	−1.10	−0.06
C4—C5	1.374	1.399	C4—C3—C2	118.72	118.14	C2—C3—C4—C5	0.10	0.02
C5—C6	1.381	1.387	C5—C4—C3	121.23	120.61	C3—C4—C5—C6	0.70	0.04
C7—N1	1.295	1.290	C4—C5—C6	121.34	121.09	C4—C5—C6—C1	−0.30	−0.02
C7—N2	1.353	1.368	C5—C6—C1	117.90	119.21	C2—C1—C6—C5	−0.80	0.02
C7—S1	1.752	1.789	N1—C7—N2	122.47	125.29	S1—C1—C6—C5	−179.29	−179.61
N2—N3	1.379	1.370	N1—C7—S1	119.68	116.02	N1—C7—N2—N3	−179.94	−174.43
N2—C8	1.476	1.483	C7—N2—N3	120.77	120.23	S1—C7—N2—N2	0.02	5.20
C8—C16	1.514	1.517	C7—N2—C8	125.03	125.80	N1—C7—N2—C8	9.20	−4.60
C8—C9	1.539	1.552	N3—N2—C8	113.64	113.26	S1—C7—N2—C8	−170.80	−174.60
C10—N3	1.286	1.285	N2—C8—C16	112.30	113.30	C7—N2—C8—C16	66.85	73.63
C10—C11	1.468	1.463	N2—C8—C9	100.07	101.20	N3—N2—C8—C16	−104.54	−116.012
C10—C9	1.504	1.508	C16—C8—C9	112.80	113.42	C7—N2—C8—C9	−173.20	−164.59
C11—N4	1.336	1.342	N3—C10—C11	113.86	113.93	N3—N2—C8—C9	15.41	5.70
C11—C12	1.381	1.401	C11—C10—C9	124.95	124.08	N3—C10—C11—N4	−167.26	179.23
N4—C15	1.343	1.333	N4—C11—C12	123.07	122.61	C9—C10—C11—N4	12.10	0.23
C15—C14	1.360	1.389	N4—C11—C10	115.58	115.66	N3—C10—C11—C12	10.40	−0.50
C14—C13	1.377	1.382	C12—C11—C10	121.31	121.72	C9—C10—C11—C12	−170.21	−179.49
C13—C12	1.373	1.383	C11—N4—C15	116.20	117.96	C12—C11—N4—C15	−1.70	0.00
C16—C17	1.384	1.393	N4—C15—C14	124.55	123.49	C10—C11—N4—C15	175.96	−179.73
C16—C21	1.388	1.394	C15—C14—C13	118.37	118.29	C11—N4—C15—C14	0.50	−0.02
C17—C18	1.387	1.390	C12—13—14	118.74	119.06	N4—C15—C14—C13	1.30	0.03
C18—C19	1.378	1.387	C17—C16—C21	118.71	118.74	N2—C8—C16—C17	−142.10	−147.55
C19—C20	1.370	1.388	C17—C16—C8	119.91	119.71	C9—C8—C16—C17	105.70	97.79
C19—Cl1	1.745	1.756	C21—C16—C8	121.30	121.48	N2—C8—C16—C17	41.38	35.31
C20—C21	1.379	1.389	C16—C17—C18	121.07	121.08	C9—C8—C16—C21	−70.83	−79.33
			C19—C18—C17	118.59	119.05	C21—C16—C17—C18	0.30	0.40
			C19—C20—C18	121.51	120.87	C8—C16—C17—C18	0.00	−0.20
			C20—C19—Cl1	119.10	119.51	C17—C18—C19—C20	−0.40	−0.08
			C18—C19—Cl1	119.39	119.51	C17—C18—C19—Cl1	−179.63	−179.72
			C19—C2—C21	119.34	119.29	C18—C19—C20—Cl1	0.50	0.20
			C20—C21—C16	120.78	120.84	CL1—C19—C20—C21	179.71	179.89
			C7—N1—C2	109.01	110.93	C19—C20—C21—C26	−0.20	−0.04
			C10—C9—C8	102.23	102.15	C17—C16—C21—C20	−0.30	−0.20
			C10—N3—N2	107.50	109.03	C8—C16—C21—C20	176.30	176.88
			C13—C12—C11	119.02	118.55	N2—C7—N1—C2	178.79	−179.421
			C1—S1—C7	87.58	87.90	S1—C7—N1—C2	−1.16	0.20
						C3—C2—N1—C7	−179.24	179.95
						C1—C2—N1—C7	0.19	0.102
						N3—C10—C9—C8	12.21	5.12
						C11—C10—C9—C8	−167.17	−175.81
						N2—C8—C9—C10	−15.02	−5.93
						C16—C8—C9—C10	104.52	115.75
						C11—C10—N3—N2	176.52	179.23
						C9—C10—N3—N2	−2.89	−1.67
						C7—N2—N3—C10	179.54	168.07
						C8—N2—N3—C10	−8.66	−2.87
						C14—C13—C12—C11	0.80	0.00
						N4—C11—C12—C13	1.10	0.00
						C10—C11—C12—C13	−176.45	179.72
						C6—C1—S1—C7	177.47	179.98
						C2—C1—S1—C7	−1.12	0.4
						N1—C7—S1—C1	1.39	−0.40
						N2—C7—S1—C1	178.56	179.28

C26, the experimental values are at (18.98) ppm while calculated values are at (133.16) ppm and (130.12) ppm respectively. Similarly for C15 and C3, the experimental values are at (152.31) ppm and the corresponding calculated values are at (158.43) ppm and (154.64) ppm respectively. The detailed values for calculated ^{1}H and ^{13}C NMR chemical shifts of the title compound together with the corresponding experimental values are shown in Table 2 and Table 3 as values relative to tetramethylsilane.

UV–Vis studies and electronic properties

In the present study we have used the fully optimized ground state geometry of the title compound to find the excited states. These states include both triplet as well as singlet states. We have computed the electronic spectra of the title compound using THF as solvent. The electronic spectrum is recorded within the range 200–800 nm. We have calculated the excitation energies and the

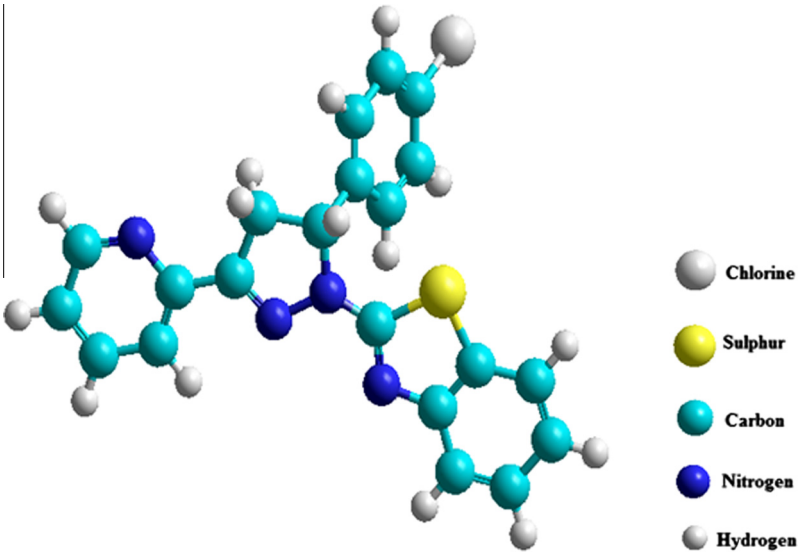

Fig. 1. Structure of title compound using Hyperchem.

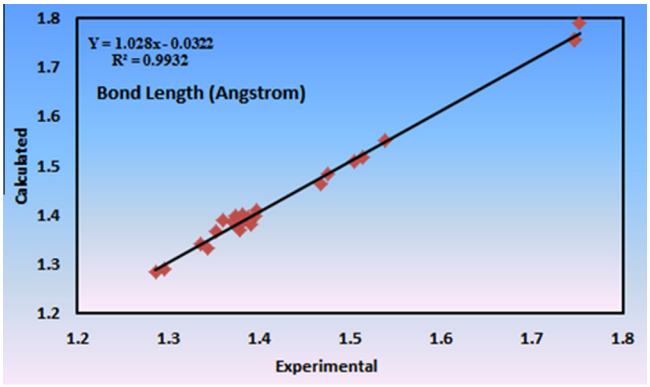

Fig. 2. Correlation between the calculated and the experimental values of the bond length for stable conformation of the title compound.

oscillator strength for the singlet and triplet states using TD-DFT approach with B3LYP level of theory using 6-311++G(2d,2p) basis set. The different values for excitation energy along with CI expansion coefficients and oscillator strength are listed in Table 4. The UV–Vis spectrum of the title compound is shown in Fig. 3. We can usually comment upon different type of electronic transitions according to the orbitals responsible for them like π–π^*, n-π^* and acceptor(π^*)-donor(π) type of transitions. The maximum absorption value obtained for the title compound using TD-DFT/B3LYP/6-311++G(2d,2p) basis set are 385 nm with THF as solvent while the corresponding experimentally calculated values as reported by other authors is 354 nm for THF. The calculated band observed at 384 nm is intense and accounts for a π–π^*transistion. λ_{max} absorption band in the calculated spectrum indicates a HOMO(101) → LUMO(102) transition and is in well agreement with the experimentally calculated values.

Table 3
Comparison of B3LYP/6-311++G(2d,2p) calculated and experimental values Ref [1]* of ^{13}C chemical shift (ppm) relative to the TMS for the title compound.

	Experimental	(B3LYP/6-311++G(2d,2p)
C12	162.89	167.94
C7	153.93	159.24
C15, C3	152.31	158.43, 154.64
C5	150.41	158.03
C24	149.37	154.64
C21	139.59	147.15
C11	43.29	46.60
C10	63.41	69.33
C25	131.69	134.70
C22, C26	128.98	133.16, 130.12
C19	125.76	129.78
C2	124.09	127.64
C6	122.17	126.11
C18	121.36	125.40
C20	120.80	124.27
C17	120.30	124.06

Molecular electrostatic potential

To understand the hydrogen bonding interactions as well as sites for nucleophilic and electrophilic attacks [19,20] molecular

Table 2
Comparison of B3LYP/6-311++G(2d,2p) calculated and experimental values Ref [1]* of ^{1}H chemical shift (ppm) relative to the TMS for the title compound.

	Experimental value		B3LYP/6-311++G(2d,2p)
H30	8.58–8.60	(m, 1H, Ar CH)	9.00
H31	8.17–8.19	(m, 1H, Ar CH)	8.99
H28	7.76	(d,1H, Ar CH)	8.19
H38	7.65	(m,1H, Ar CH)	8.11
H35	7.54	(d,1H, Ar CH)	7.96
H40,H41,H39,H42,H36,H37	7.25–7.32	(m, 6H, Ar CH)	7.47–7.89
H29	7.09–7.14	(m,1H,Ar CH)	7.65
H32	5.80	(d,d, 1H,Pyrazoline-H)	5.58
H34	4.05	(d,d,1H,Pyrazoline-H)	4.31
H33	3.49	(d,d,1H,pyrazoline-H)	3.47

Table 4
Calculated electronic absorption spectrum of 2-(5-(4-Chlorophenyl)-3-(pyridin-2-yl)-4,5-dihydropyrazol-1-yl)benzo[d]thiazole using TD-DFT/B3LYP/6-311++G(2d,2p),with experimentally reported values by other authors are in brackets.

Excited state (triplet/singlet)	CI expansion coefficient	Energy (eV)	Wavelength calc. (nm)	Oscillator strength (f)
1(T)				
98 → 102	0.19766	2.3439	528.96	0.0000
101 → 102	0.65304			
2(S)				
101 → 102	0.70468	3.2425	382.87 (354)	0.7457
3(T)				
98 → 102	−0.26123	3.3565	369.39	0.0000
99 → 102	−0.14932			
100 → 102	−0.15101			
100 → 106	−0.22100			
100 → 107	0.12416			
101 → 106	0.38437			
101 → 107	0.30681			
4(T)				
96 → 105	−0.20484	3.6299	341.57	0.0000
97 → 104	0.13860			
97 → 105	−0.26619			
98 → 104	−0.11893			
98 → 105	−0.11352			
99 → 102	−0.10097			
99 → 103	0.22887			
99 → 104	0.38621			
99 → 105	0.18477			
99 → 108	0.12177			
100 → 104	−0.13812			
5(T)				
94 → 102	−0.14761	3.7447	331.09	0.0000
94 → 103	−0.16649			
98 → 102	−0.20549			
98 → 103	0.19296			
100 → 106	0.14431			
101 → 102	0.13842			
101 → 103	0.38127			
101 → 104	−0.26708			
101 → 107	−0.10029			
6(T)				
93 → 102	−0.11050	3.8688	320.47	0.0000
98 → 102	0.19015			
98 → 107	−0.13447			
99 → 102	0.11880			
100 → 102	0.26267			
100 → 107	0.13714			
101 → 103	0.37182			
101 → 105	0.13623			
101 → 106	−0.13644			
101 → 107	0.31385			
7(T)				
93 → 102	0.10601	3.8812	319.44	0.0000
98 → 102	−0.24012			
100 → 102	0.43799			
100 → 106	0.23048			
101 → 103	−0.28358			
101 → 107	0.21497			
8(T)				
98 → 106	−0.11416	3.9619	312.94	0.0000
100 → 102	0.28294			
100 → 106	0.12388			
101 → 103	0.15416			
101 → 104	0.15487			
101 → 105	−0.16824			
101 → 106	0.45732			
101 → 107	−0.22940			
9(T)				
96 → 102	0.35607	3.9847	311.15	0.0000
96 → 103	0.14192			
97 → 102	−0.24852			
98 → 102	−0.12140			
100 → 102	−0.11204			
101 → 103	0.11374			
101 → 104	0.41708			
10(T)				
96 → 102	−0.35789	3.9904	310.71	0.0000
96 → 103	−0.14430			

(*continued on next page*)

Table 4 (*continued*)

Excited state (triplet/singlet)	CI expansion coefficient	Energy (eV)	Wavelength calc. (nm)	Oscillator strength (f)
97 → 102	0.27664			
97 → 103	0.10251			
100 → 102	−0.13823			
101 → 103	0.11246			
101 → 104	0.39244			
101 → 106	−0.10936			
11(S)				
101 → 103	0.43725	4.0163	308.70	0.0155
101 → 104	0.53889			
12(S)				
100 → 102	0.67915	4.0834	300.40	0.0114
101 → 107	−0.10900			
13(S)				
101 → 103	0.53944	4.1272	300.40	0.0127
101 → 104	−0.43892			
14(T)				
100 → 102	−0.22328	4.1619	297.90	0.0000
100 → 106	0.33617			
100 → 107	−0.32853			
101 → 104	−0.10179			
101 → 106	0.12826			
101 → 107	0.30663			
15(S)				
101 → 105	0.69647	4.2067	294.73	0.0025
16(S)				
96 → 102	0.48411	4.3954	282.08	0.0107
97 → 102	−0.35716			
99 → 102	0.33393			
17(S)				
96 → 102	−0.26157	4.4441	278.99	0.0804
97 → 102	0.19864			
99 → 102	0.53288			
101 → 106	0.28098			
101 → 107	−0.10125			
18(S)				
99 → 102	−0.30005	4.5074	275.07	0.0816
100 → 102	−0.13051			
100 → 106	0.10620			
100 → 107	0.14447			
100 → 106	0.47040			
101 → 107	−0.32546			
19(S)				
98 → 102	0.43285	4.5719	271.19	0.2643
101 → 106	0.26675			
101 → 106	0.46602			
20(S)				
101 → 108	0.60887	4.6626	265.91	0.0019
101 → 109	0.27510			
101 → 112	−0.10172			

electrostatic potential surface map of the title compound is investigated using B3LYP/6-311++G(2d,2p) level of theory. This surface provides us a net electrostatic effect caused due to total charge distribution along with an idea to comment upon the polarity of the molecule. Different colours are used to indicate the values of electrostatic potential at the surface of the molecule. The colors used are red, orange, green, blue and the order for increase in the value of electrostatic potential is red < orange < yellow < green < blue. The MEP surface map for the title compound is shown in Fig. 3 (Supplementary information). From the MEP surface we conclude that title compound had possible sites for electrophilic as well nucleophilic attack. The range of the potential is from −5.567 kcal/mol to +5.567 kcal/mol with reddish and yellowish areas related to nucleophilic reactivity concentrated over nitrogen atom while the bluish regions to nucleophilic reactivity concentrated over benzene ring attached to chlorine atom. From this we conclude that the most reactive sites of the title compound are the sites containing the nitrogen atom.

Vibrational analysis

We have investigated the molecular vibrations of the title compound by means of FT-IR spectroscopy. The title compound consists of 42 atoms, belongs to C1 point group and have 120 normal modes of vibrations. The assignments of the fundamental modes of vibration of the title compound are investigated using B3LYP/6-311++G(2d,2p) level of theory with Gaussian 09 program. The calculated IR spectra of the title compound is shown in Fig. 4. The experimental values for the absorption bands in the IR spectra as reported by other authors occur at IR(cm^{-1}): 3053, 2987, 2921, 1755, 1724, 1459, 1421, 1261, 1150, 757, and 692 respectively while the calculated values using B3LYP/6-311++G(2d,2p) level of theory are at IR(cm^{-1}): 3057, 3194, 1630,1585, 1482, 1277, 1140, 1037, 855, 752, 558, 421, 170, and 102 respectively. By looking at the experimental and calculated values we can say that they are in close agreement with each other. We have also reported the PED analysis of the title compound which is given in Table 5.

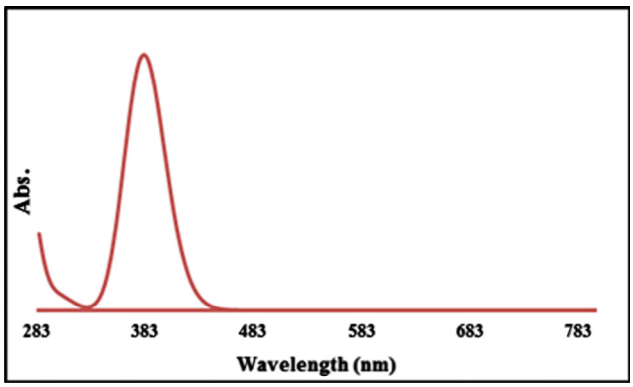

Fig. 3. UV–Vis spectrum of 2-(5-(4-Chlorophenyl)-3-(pyridin-2-yl)-4,5-dihydropyrazol-1-yl)benzo[d]thiazole.

Larger is the molecule under study more important is PED analysis methodology. In our system we have 120 modes of vibrations each, all of them is described by a normal mode coordinate, which in the PED is expressed in terms of internal mode contributions. Each of the internal coordinate is expressed as a superposition of various local modes two, three, or four atoms connected by bonds [21]. In this procedure, a normal coordinate of a molecule is transformed into an internal coordinate, which is a combination of stretching's, bending's, or torsions. This transformation basically results in the non-diagonality of the force constant matrix, which means that PED contributions of different modes are mutually related to each other by non-diagonal terms. This procedure is followed as: The set of coordinate is replaced by an internal set of coordinate and the PED's are calculated. The sum of the absolute values of maximum PED's for each of the modes is expressed by a parameter EPm. This procedure is basically known as optimization of the PED analysis. Optimization times generally increases with an increase in the number of modes. The IR spectra is analyzed in terms of the PED contributions by using the VEDA program [22]. During this analysis we found that the title compound has 120 modes of vibrations out of which 41 are stretching, 40 bending, 34 torsion, 5 out of plane modes respectively.

Ring vibrations and CH_2 group vibrations-

The C-H stretching vibrations of aromatic compounds generally occur in the range from 2800 to 3100 cm^{-1}[23]. In our title compound these vibrations using DFT/B3LYP/6-311 + G(2d,2p) generally occurs at 3157–3212 cm^{-1} respectively. As experimentally reported by other authors the values at 3057 and 3194 cm^{-1} for title compound correspond to C—H stretching vibrations. From the PED analysis we found that they are pure modes as their percentage mostly varies from 90% to 99%. C—H stretching vibrations of the title compound are also predicted in range from 3049 to 3212 cm^{-1} using DFT level of theory. The benzene ring C-H bending vibrations for the title compound are observed in the range from 1297 to 1613 cm^{-1} respectively, however the vibrations for the title compound observed at values 1613, 1528, 1504,1490, 1349–1471 cm^{-1} respectively are mixed with stretching C—C and C—N vibrations. The C—Cl absorption generally occurs in a broad range from 800 to 600 cm^{-1}. The mode no (52, 97, 102, 104) in Table 5 for PED distribution of the title compound are assigned to C—Cl modes and the corresponding wavenumbers are 297, 333, 427, 1102 cm^{-1} respectively. These modes are mixed with C—H bending modes. The C—C stretching vibrations for the title compound calculated by DFT theory occurs in the range from 1083 to 1633 cm^{-1} respectively and are mixed with bending and torsional modes of vibrations. In our title compound we have three 6-membered and two 5-membered rings, out of which for C—C vibrations the strongest one is at 1258 cm^{-1}. The C—C stretching vibrations [24] for ring 4 occur at 1297 and 1596 cm^{-1} respectively. The values observed at 3116 and 3074 cm^{-1} are assigned to symmetric stretching bands of methyl hydrogens [25]. The percentage of PED calculated by VEDA 4 program for these modes varies from 80% to 90%.

C—N, C—S and N—N group vibrations

We have assigned the C—N modes of vibrations on the basis of PED calculations. The calculated band using DFT theory at 1641 cm^{-1} is assigned to C—N stretching modes [26]. It is pure mode and its PED contribution is around 53%. The bands at 1616, 1569, 1404 cm^{-1} are also assigned to C—N stretching modes. These modes are mixed with other bending modes. The PED contribution for mode no 19 is around 59%. The C—N stretching modes at mode no 17 and 31 are coupled with stretching and bending mode of vibrations. On the basis of PED analysis, the absorption band at 1081 and 507 cm^{-1} are assigned to the C—S group vibrations. The mode no 53 at absorption band 1081 has PED contribution around 18%. The mode at 507 cm^{-1} is mixed with bending mode of vibrations. The prominent peaks at values 1012, 996, 968, 826, 712, 681, and 507 are assigned to N—N stretching vibrations. The

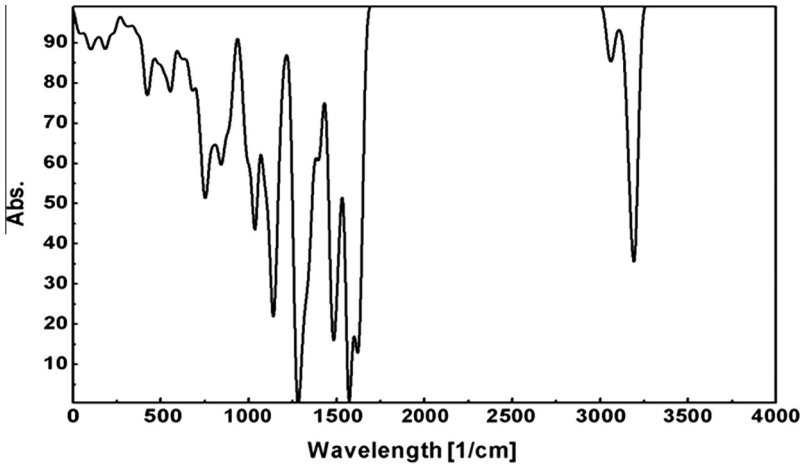

Fig. 4. Calculated IR spectra of the title compound at B3LYP/6-311 + G(2d,2p) level.

Table 5
Vibrational wavenumbers obtained for the title compound at B3LYP/6-311++G(2d,2p) method.

Normal mode No.	Calculated wavenumbers (cm^{-1})	IR_{Int}	PED (%)	Interpretation
1	3212.94	2.13	s3 92	υ_sCH,ring1
2	3211.17	0.51	s5 85 s6 10	υ_sCH,ring5
3	3210.32	1.86	s14 92	υ_sCH,ring5
4	3203.14	13.6	s13 95	υ_sCH,ring4
5	3199.46	15.39	s2 14 s4 79	υ_sCH,ring1
6	3196.88	16.04	s10 96	υ_sCH,ring4
7	3185.63	5.85	s11 99	υ_sCH,ring4
8	3185.52	1.82	s6 83	υ_sCH,ring5
9	3180.59	6.49	s2–81 s4–14	υ_sCH,ring1
10	3174.56	2.1	s12 96	υ_{as}CH,ring4
11	3170.15	6.41	s15 89	υ_sCH,ring5
12	3157.31	27.05	s1 95	υ_sCH,ring1
13	3116.25	2.75	s8–88	$\upsilon_{as}CH_2$,ring2
14	3074.37	9.06	s8–10 s9 82	υ_sCH_2,ring2
15	3049.2	9.56	s7 89	υ_sCH,ring2
16	1641.01	45.32	s19 53	υCN
17	1634.81	68.99	s18–14 s20 12 s31–32	υCN,ring3 + υCC,ring4
18	1633.95	9.08	s30–56 s61 16	υCC,ring5 + βHCC,ring5
19	1616.47	109.02	s16 59	υCN,ring2
20	1613.09	0.95	s29 62 s51 13	υCC,ring5 + βHCC,ring5
21	1601.1	30.34	s26 54 s50–12	υCC,ring1 + βHCC,ring1
22	1596.91	23.63	s32 51	υCC,ring4
23	1569.24	809.83	s18–64	υCN,ring3
24	1528.81	64.42	s60 64 s66 10	βHCC,ring5 + βCCC,ring5
25	1504.89	124.95	s24 18 s26–13 s49 27 s50–10	υCC,ring4 + βCCC,ring5
26	1490.34	26.98	s20 14 s31 18 s57 49	υCC,ring4 + βHCC,ring4
27	1485.53	6.56	s55 90	βHCH,ring2
28	1475.45	18.98	s59 33	βHCC,ring4
29	1471.93	150.87	s47–12 s50–13 s59 14	βHCC,ring1
30	1444.42	15.48	s28–25 s51–10 s52–22 s54 17	υCC,ring5 + βHCC,ring5
31	1404.88	107.87	s33 19 s50 17	υCN,ring2 + βHCC,ring2
32	1374.52	39.27	s21 12 s52 17 s54 43	υCC,ring5 + βHCC,ring2
33	1349.08	89.77	s33 14 s88 17	υCN,ring2 + τHCCC,ring5
34	1337.06	46.74	s27 50 s56 10	υCC,ring4 + βHCC,ring4
35	1328.34	5.94	s51–67	βHCC,ring5
36	1315.93	20.22	s17 10 s49 28	υCC,ring2 + βHCN,ring1
37	1311.58	41.96	s49 12 s58–12	βHCN,ring3 + βHCC,ring4
38	1297.98	15.03	s21 45 s73–10	υCC,ring4 + βCCC,ring5
39	1292.85	67.91	s23–57 s88 11	υCN,ring1 + τHCCC,ring3
40	1278.81	3.89	s31 19 s34–14 s58–31	υCN,ring 3 + βHCC,ring4
41	1275.78	225.89	s23–15 s35–12 s88–27	υCC + υCN,ring1 + τHCCC,ring2
42	1258.72	104.33	s33–14 s89–40	υCN,ring3 + τHCCC,ring2
43	1217.58	2.59	s21–10 s38 33 s54 13 s60 12	υCC,+ βCCC,ring5
44	1205.68	2.44	s30 22 s61 73	υCC,+ βHCC,ring5
45	1183.14	0.35	s32 11 s56–66	υCC,+ βHCC,ring4
46	1176.02	19.05	s23–15 s48 66	υCN,+ βHCC,ring1
47	1167.47	12.1	s53 52 s90–15	βHCC + τHCCC,ring2
48	1147.64	105.94	s20 23 s37–10 s57–18 s58 16	υCN,ring 2 + βHCC,ring5
49	1139.68	40.99	s20 11 s37 12 s52 11	υCN,ring 2 + βHCC,ring5
50	1131.33	50.92	s28 19 s52–36	υCC,ring 5 + βHCC,ring5
51	1120.18	2.76	s17–22 s47–49	υCC,ring 5 + βHCC,ring5
52	1102.01	64.53	s22 44 s41 26 s60 13	υCLC,+βHCC,ring5
53	1081.69	38.11	s40 18 s72 52	υSC,ring3 + βCCC,ring4
54	1072.01	1.53	s24 29 s50 16	υCC + βHCC,ring1
55	1049.63	13.91	s24 11 s71 32	υCC + βCNC,ring4
56	1038.63	15.64	s25 54 s59 22	υCC + βHCC,ring4
57	1035.41	41.25	s66 80	βCCC,ring5
58	1029.87	17.08	s53 11 s78 16 s90 10 s120–11	βHCC,ring1 + βNNC,ring2 + τHCCC,ring4 + ϕCCCC
59	1021.98	0.18	s84 79	τHCCC,ring1
60	1012.49	0.18	s24 13 s36 10 s42 23 s64 12	υNN,ring 2 + βCCC,ring1 + βCCN,ring1
61	996.47	21.32	s36 17 s44–10 s86 23	υNN,ring 2 + βCNC,ring2 + τHCCC,ring1
62	993.68	11.07	s86–54 s102–12	τHCCC,ring5 + τCCCC,ring5
63	991.43	0.06	s94 65	τHCCC,ring4
64	989	1.25	s82 72	τHCNC,ring1
65	976.94	3.47	s96 68 s109 10	τHCCC,ring5 + τCCCC,ring5
66	968.21	3.27	s78 12 s90–20	βNNC,ring2 + τHCCC,ring5
67	951.66	1.73	s91–75 s101 12	τHCCC,ring2 + τCCCC,ring3
68	916.14	0.88	s83 84	τHCCC,ring1
69	901.74	22.78	NA	NA
70	882.06	25.55	s39 51	υCN,ring 2
71	869.69	1.53	s93 83	τHCCC,ring4
72	851.38	36.84	s87–74	τHCCC,ring5
73	842.96	10.31	s87–14 s95 75	τHCCC,ring5
74	826.9	19.58	s34 14 s63–10	υNC,ring 3 + βCNN,ring2

Table 5 (*continued*)

Normal mode No.	Calculated wavenumbers (cm^{-1})	IR_{Int}	PED (%)	Interpretation
75	803.15	39.84	s85 19 s105 29	τHCCN,ring1 + τCCNC,ring2
76	788.77	5.4	s41 12 s43 24	υCC + βCCC,ring2
77	769.7	26.09	s92 19 s94 10 s110 51	τHCCC,ring5 + τCCCC,ring5
78	758.13	19	s85 55 s105–33	τHCCN,ring1 + τCCNC,ring1
70	745.93	1.62	s96 23 s109–46	τHCCC,ring5 + τCCCC,ring5
80	745.26	40.22	s92 56 s110–17	τHCCC,ring4 + τCCCC,ring5
81	722.47	15.72	s68 52	βCCC,ring1
82	712.82	3.26	s40–24 s63 19 s74 20 s75 13	υSC,ring + βCNN + βCCS
83	681.79	9.04	s63 16 s65–31 s74 13	βCNN,ring2 + βCNN,ring2
84	675.77	11.6	s22 10 s73–16 s79 28	υClC + βCCC,ring5 + βCCN,ring1
85	645.6	0.75	s29 14 s67–69	υCC + βCCC,ring5
86	636.03	5.75	s42 21 s64 27 s69–26	βCCC,ring5 + βCCN,ring1 + βCCC,ring4
87	615.28	1.29	s108 57 s112–17	τCNCC,ring1 + τCCCC,ring4
88	602.81	5.19	s46–38	βCCC,ring4
89	562.07	5.41	s112–12 s120 11	τCCCC,ring4 + ϕCCCC,ring5
90	561.8	4.8	s97 32 s104–15	τCCCN,ring1 + τCCCN,ring3
91	553.16	4.84	s108–14 s112 32	τCNCC,ring1 + τCCCC,ring4
92	523.36	14.49	NA	NA
93	507.32	0.95	s40 21 s63 12 s70–45	υSC + βCNN,ring2 + βCCN,ring3
94	483.5	13.24	NA	NA
95	456.37	1.2	s118 14	ϕCCCC,ring5
96	440.43	5.93	s91 13 s92 13 s101 60	τHCCC,ring4 + τCCCC,ring5
97	427.39	2.35	s45–11 s109 10 s116–13	βCCN,ring1 + τCCCC,4ring + ϕCLCC
98	420.71	0.1	s86 19 s102–74	τHCCC,ring5 + τCCCC,ring5
99	417.42	4.83	s82 12 s100 64	τHCNC,ring1 + τCCNC,ring3
100	411.93	5.11	s75 14	βCCS,ring3
101	370.01	4.8	s75 10	βCCS,ring3
102	333.29	1.24	s80–13 s81 23 s117 11	βCCC,ring5 + βCLCC + τCCCN,ring1
103	314.08	0.41	s81 31 s117–15	βCLCC + τCCCN,ring1
104	297.31	0.65	s78 10 s116 20	βNNC,ring2 + ϕCLCC
105	284.44	0.28	s113 28 s117 17	τCCNN,ring2 + τCCCN,ring1
106	238.94	3.43	s44 14	βCNC,ring2
107	214.57	0.96	s35–11	υCC
108	188.78	1.32	s106 63	τCCCC,ring4
109	187.39	1.35	s118–21	ϕCCCC,ring4
110	176.48	1.63	s80 29 s99 13	βCCC,ring4 + τCNCN,ring2
111	142.77	4.1	s76–41	βCCN,ring1
112	108.81	1.98	s80–17 s111–21	βCCC,ring1 + τCNCC,ring2
113	107.03	1.94	s98–15 s104–10 s111 18 s113 10	τCNCC,ring1 + τCCCN,ring2 + τCNCC,ring3 + τCCNN,ring1
114	83	3	s103 46 s107 16S	τCNCN,ring2 + τNCCN,ring3
115	53.85	0.96	s62 71	βCCN,ring2
116	38.8	0.75	s107 63	τNCCN,ring1
117	34.84	0.01	s115 71	τCCCN,ring2
118	29.33	0.55	s119–72	τCCCN,ring3
119	18.77	0.02	s99 51	τCNCN,ring2
120	14.09	0.02	s98 30 S114 45	τCNCC,ring2 + τNNCC,ring3

υ, β, τ, ϕ denotes the stretching, bending, torsion and out(τ ABCD means dihedral angle between ABC and BCD planes, ϕ ABCD means the angle between the AD vector and the BCD plane) modes. Indices notation : s, symmetric; a, asymmetric; υ, stretching: ring1: N4—C5—C6—C1—C2—C3, ring2: C11—C7—N8—N9—C20, ring3:-N16—C15—C14—S13—C12, ring4:C14—C15—C20—C19—C18—C17, ring 5:C21—C22—C23—C24—C25—C26.

PED contribution for 1012 and 996 cm^{-1} are around 23% and the bands at other values have mixed contribution from other modes of vibrations.

NBO analysis

We have reported the NBO analysis of the title compound using NBO 3.1 program implemented in Gaussian 09 package using DFT/B3LYP/6-311++G(2d,2p) level of theory in order to understand the hyper conjugation as well as delocalization. From the NBO analysis we can investigate the charge transfer conjugative interaction in molecular systems. NBO method provide us information about the interactions of both filled and virtual orbital spaces which can be further helpful in the analysis of both inter and intramolecular interactions. We have reported the second order Fock-order analysis of the title compound at DFT/B3LYP/6-311++G(2d,2p) level of theory to analyze the donor acceptor interactions. The stabilization energy (E_2) for each donor (i) and acceptor (j) associated with the delocalization $i \rightarrow j$ is determined as

$$E(2) = \Delta E_{ij} = q_i \frac{(F_{ij})^2}{(E_j - E_i)}$$

where $q_i \rightarrow$ donor orbital occupancy, E_i, $E_j \rightarrow$ diagonal elements, $F_{ij} \rightarrow$ off diagonal NBO Fock matrix element. As per above equation larger value of $E(2)$ means greater is the interaction between the electron-donors and electron-acceptor, and greater is the extent of conjugation. The possible interactions between different type of NBO's are listed in Table 6. In the NBO analysis of the title compound we found that the overlap between C—C, C═N, N—N and C—S bonding and antibonding orbitals causes stabilization of the title compound. From the Table 6, we can say that the intermolecular hyper conjugative interaction of σ (C17—C18) distributes to σ*(S13—C14), (C14—C17) leading to stabilization of (4.17–6.13) kcal mol^{-1}. From Table 6, we can see similar kind of interactions for (C25—C26) and (C21—C26) bond lengths. The most important interaction energies of LP(3)CL27 → π*(C23—C24), LP(2)S13 → π* (C12—N16), LP(1)N9 → π*(C12—N16) are 12.02, 25.23 and 51.16 kcal mol^{-1} respectively. The magnitude of charge transfer

from the lone pairs of N4, N8, N9 to antibonding (C25—C26), (C7—C11), (C5—C6) σ orbitals leads to stabilization of 14.41, 8.50, 20.37 kcal mol^{-1} respectively. The delocalization of electron σ(C21—C26) to σ^*(C22—C23), σ^*(C25—C26) and σ(C25—C26) to σ^*(C25—C26) leads to tremendous stabilization energy of 98.54, 603.20, and 1303.04 kcal mol^{-1} respectively.

Conclusions

Using DFT/B3LYP/6-311++g(2d,2p) level of theory we have reported the detailed study of structural, vibrational, PED analysis, NMR (^{13}C and ^{1}H) electronic and reactivity of the title compound. We have also compared our calculated values with experimental results obtained by other authors and found that they are in close agreement to each other. We have seen in our HOMO–LUMO calculations that the charge transfer occurs through π system which may accounts for the bioactivity of the title compound. Molecular electrostatic surface maps give an idea about the chemical reactivity of the title compound. Our overall simulated results for different molecular properties of the title compound are obtained for the first time and we hope that they are helpful in the synthesis and design of new applications.

Table 6
Second order Perturbation theory analysis of Fock matrix basis in NBO basis.

Donor (i)	Type	ED/e	Acceptor (j)	Type	ED/e	$E(2)$[a] (kcal mol^{-1})	$E(j)-E(i)$[b] (a.u)	$F(i,j)$[c] (a.u)
C1—C6	π	1.65243	C2—C3	π^*	0.29948	17.82	0.28	0.064
C1—C6	π	1.65243	N4—C5	π^*	0.44057	26.80	0.26	0.077
C2—C3	π	1.63730	C1—C6	π^*	0.27485	20.80	0.29	0.071
C2—C3	π	1.63730	N4—C5	π^*	0.44057	16.72	0.26	0.061
N4—C5	π	1.70377	C1—C6	π^*	0.27485	12.25	0.33	0.057
N4—C5	π	1.70377	C2—C3	π^*	0.29948	26.23	0.32	0.082
N4—C5	π	1.70377	C7—N8	π^*	0.20471	13.69	0.32	0.060
C7—N8	σ	1.90739	N4—C5	σ^*	0.44057	10.86	0.33	0.059
N8—N9	σ	1.98043	C5—C7	σ^*	0.04068	4.27	1.29	0.067
C12—S13	σ	1.97298	N8—N9	σ^*	0.3153	5.25	0.99	0.064
C12—N16	π	1.98043	C14—C15	π^*	0.48019	17.63	0.35	0.077
C14—C15	π	1.63134	C12—N16	π^*	0.39957	9.91	0.26	0.045
C14—C15	π	1.63134	C17—C18	π^*	0.34224	20.97	0.29	0.070
C14—C15	π	1.63134	C19—C20	π^*	0.31711	13.26	0.27	0.054
C14—C17	σ	1.97739	C14—C15	σ^*	0.04297	4.20	1.26	0.065
C15—N16	σ	1.97642	N9—N12	σ^*	0.04778	6.99	1.22	0.083
C15—C20	σ	1.97019	C14—C15	σ^*	0.04297	4.58	1.23	0.067
C17—C18	σ	1.97109	S13—C14	σ^*	0.02748	6.13	0.90	0.066
C17—C18	σ	1.97109	C14—C17	σ^*	0.02127	4.17	1.27	0.065
C17—C18	π	1.69862	C14—C15	π^*	0.48019	17.66	0.27	0.065
C17—C18	π	1.69862	C19–20	π^*	0.31711	20.16	0.26	0.065
C19—C20	σ	1.97666	C15—N16	σ^*	0.02116	4.67	1.17	0.066
C19—C20	π	1.70012	C14—C15	π^*	0.48019	21.18	0.27	0.071
C19—C20	π	1.97813	C17—C18	π^*	0.34224	19.21	0.28	0.066
C21—C22	π	1.65928	C23—C24	π^*	0.38687	21.42	0.27	0.069
C21—C26	σ	1.97048	C17—C18	σ^*	0.01495	5.63	1.30	0.031
C21—C26	σ	1.97048	C19—C20	σ^*	0.01352	26.59	1.29	0.166
C21—C26	σ	1.97048	C19—C20	π^*	0.31711	41.14	0.73	0.167
C21—C26	σ	1.97048	C22—C23	σ^*	0.01569	98.54	1.17	0.305
C21—C26	σ	1.97048	C23—C24	σ^*	0.02813	60.85	1.24	0.245
C21—C26	σ	1.97048	C24—C25	σ^*	0.02821	73.74	2.16	0.356
C21—C26	σ	1.97048	C25—C26	σ^*	0.01577	603.20	1.50	0.852
C21—C26	σ	1.97048	C25—C26	π^*	0.31392	5.38	5.44	0.165
C23—C24	π	1.67586	C21—C22	π^*	0.35369	17.05	0.32	0.067
C25—C26	σ	1.96872	C10—c11	σ^*	0.01901	12.94	1.05	0.104
C25—C26	σ	1.96872	C19—C20	σ^*	0.01352	21.72	1.28	0.150
C25—C26	σ	1.96872	C19—C20	π^*	‘0.31711	30.59	0.73	0.144
C25—C26	σ	1.96872	C22—C23	π^*	0.1569	73.13	1.17	0.269
C25—C26	σ	1.96872	C23—C24	σ^*	0.02813	49.47	1.23	0.221
C25—C26	σ	1.96872	C24—C25	σ^*	0.02821	85.31	2.15	0.383
C25—C26	σ	1.96872	C25—C26	σ^*	0.01577	1303.04	1.50	1.251
C25—C26	π	1.66232	C21—C22	π^*	0.35369	17.94	0.30	0.066
C25—C26	π	1.66232	C23—C24	π^*	0.38687	20.47	0.27	0.067
C25—C26	π	1.66232	C24—C25	σ^*	0.02821	13.32	1.70	0.146
C25—C26	π	1.66232	C24—CL27	σ^*	0.03312	16.49	1.24	0.139
LP(1)N4	σ	1.91989	C2—C3	σ^*	0.02522	8.97	0.90	0.081
LP(1)N4	σ	1.91989	C5—C6	σ^*	0.03355	10.37	0.88	0.086
LP(1)N8	σ	1.91989	C7—C11	σ^*	0.03464	8.50	0.80	0.074
LP(1)N8	σ	1.91989	N9—C10	σ^*	0.05170	8.10	0.71	0.068
LP(1)N9	σ	1.65694	C7—N8	σ^*	0.20471	24.61	0.29	0.078
LP(1)N9	σ	1.65694	C12—N16	π^*	0.39957	51.16	0.28	0.078
LP(1)N9	σ	1.65694	C25—C26	σ^*	0.01577	14.41	1.06	0.121
LP(2)S13	π	1.71928	C12—N16	π^*	0.39957	25.23	0.25	0.073
LP(2)S13	π	1.71928	C14—C15	π^*	0.48019	15.96	0.28	0.062
LP(1)N16	σ	1.87006	C12—S13	σ^*	0.08861	18.71	0.51	0.088
LP(1)N16	σ	1.87006	C14—C15	σ^*	0.04297	6.90	0.89	0.072
LP(3)CL27	n	1.92740	C23—C24	π^*	0.38687	12.62	0.33	0.062

[a] $E(2)$ means stabilization energy.
[b] Energy difference between the donor and acceptor NBO orbitals.
[c] $F(i,j)$ is the Fock matrix element between i and j NBO orbitals.

Acknowledgements

The authors thank Indian Institute of technology Mandi for providing infrastructure required for computational studies as well MHRD scholarships.

Appendix A. Supplementary material

Supplementary data associated with this article can be found, in the online version, at http://dx.doi.org/10.1016/j.saa.2014.02.196.

References

[1] S. Hu, S. Zhang, C. Gao, Spectrochim. Acta Part A: Molecul. Bimolecular Spectrosc. 113 (2013) 325–331.
[2] J.R. Lakowicz, Topics in Fluorescence Spectroscopy, New York, 1994.
[3] (a) P. Aisen, M. Wessling-Resnick, E.A. Leibold, Curr. Opin. Chem. Biol. 3 (1999) 200–206;
(b) R.S. Eisenstein, Annu. Rev. Nutr. 20 (2000) 627–662.
[4] D. Touti, Arch. Biochem. Biophys 373 (2000) 1–6.
[5] Berna Catikkas, Ebru Atkan, Zeynel Seferoglu, Int. J. Quantum Chem. 113 (2013) 683–689.
[6] Asha Raj, Y. Sheena Mary, C. Yohannan Panicker, Hema Tresa Varghese, K. Raju, Spectrochim. Acta Part A: Mol. Bimolecular Spectrosc. 113 (2013) 28–36.
[7] C.V. Filip, S. Miclaus, J. Mol. Struct. 744 (2005) 363.
[8] M. Kumru, V. Küçük, P. Akyürek, Spectrochim. Acta Part A: Mol. Bimolecular Spectrosc. 113 (2013) 72–79.
[9] R. John Xavier, P. Dinesh, Spectrochim. Acta Part A: Mol. Bimolecular Spectrosc. 113 (2013) 171–181.
[10] Gaussian 09, Gaussian, Wallingford CT, 2004.
[11] R. Ditchfiled, J. Chem. Phys. 56 (1972) 5688–5691.
[12] K. Wolinski, J.F. Hinton, J. Am. Chem. Soc. 112 (1990) 8251–8260.
[13] Yu Takano, K.N. Houk, JCTC 1 (2005) 70–77.
[14] E.D. Glendening, A.E. Reed, NBO version 3.1, TCL, University of Wisconsin, Madison, 1998.
[15] C. Lee, W. Yang, R.G. Parr, Phys. Rev. B 37 (1998) 785.
[16] M. Izadyar, M. Khavani, Int. J. Quantum Chem. (2014), http://dx.doi.org/10.1002/qua.24652.
[17] J. Fleming, Frontier Orbitals and Organic Chemical Reactions, John Wiley and Sons, New york, 1981.
[18] J.B. Foresman, E. Frisch, Exploring computational chemistry with Electronic Structure Methods Gaussian, Pittsburgh, 1995–96, p.118.
[19] Peter Politzer, Patricia R. Laurence, Keerthi Jayasuriya, Environ. Health Perspect. 61 (1985) 191–202.
[20] A. Pullman, B. Pullman, R. Lavery, J. Mol. Struct. 93 (1983) 85–91.
[21] J.R. Durig, M.M. Bergana, J. Raman. Spectrosc. 22 (1991) 141–154.
[22] M.H. Jamróz, J. Mol. Struct. 787 (2006) 172–183.
[23] L. Vrielynck, J.P. Cornard, Spectrochim. Acta part A 50 (1994) 2177–2188.
[24] A. Teimouri, A.N. Chermahini, Spectrochim. Acta A 72 (2009) 369–377.
[25] V. Krishnakumar, V. Balachandran, Spectrochim. Acta A 68 (2007) 845–850.
[26] M. Silverstein, G. Clayton, Spectrometric Identification of Organic Compounds, Wiley, New York, 1981.